

Heterogeneous Mn-Based Catalysts for the Aerobic Conversion of Methane-to-Methyl Trifluoroacetate

Yinjie Ji, Andrea N. Blankenship, and Jeroen A. van Bokhoven*



Cite This: ACS Catal. 2023, 13, 3896–3901



Read Online

ACCESS |

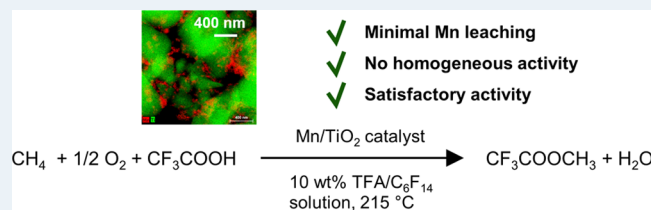
Metrics & More

Article Recommendations

Supporting Information

ABSTRACT: Methane conversion strategies that protect methanol via *in situ* esterification achieve higher yields compared to direct methane conversion without product protection; however, most of these high-yield systems operate under unfavorable conditions. To date, there is very limited work in developing heterogeneous catalysts for methane-to-methyl-ester conversion, and studies demonstrating the activity of manganese for methane conversion are limited. We have prepared a series of silica-, titania-, and zirconia-supported manganese catalysts and measured the activity of these catalysts for the aerobic conversion of methane to methyl trifluoroacetate in diluted trifluoroacetic acid. The silica-supported catalyst exhibits high overall activity, but significant amounts of homogeneously active manganese are observed. Titania- and zirconia-supported manganese catalysts catalyze the reaction heterogeneously with activities up to $613 \mu\text{mol g}_{\text{cat}}^{-1} \text{ h}^{-1}$ and show nondetectable leaching. Manganese oxide is poorly dispersed on titania and zirconia, whereas high dispersion is realized on silica. This work demonstrates a facilely synthesized supported manganese catalyst that converts methane heterogeneously in satisfactory yields under improved conditions in a diluted acid, compared to those of conventional methane-to-methyl-ester systems.

KEYWORDS: heterogeneous catalysis, methane partial oxidation, product protection, methyl trifluoroacetate, supported manganese catalysts



Methane, the major constituent of natural gas, is a highly abundant and versatile resource to produce commodity chemicals and liquid energy carriers, especially methanol.¹ The current methane utilization route proceeds through the generation of syngas with subsequent conversion to desired chemicals, which is a highly energy- and capital-intensive process and thus only economically viable for large-scale applications.² In this context, it is imperative to develop scale-flexible and syngas-free methane conversion routes. The selective oxidation of methane to liquid oxygenates has been previously demonstrated with a variety of solid catalysts in both stoichiometric and catalytic modes.³ The conversion of methane over copper-exchanged zeolites is one of the largest focuses within the field of methane conversion, with one notable advantage of these systems being the ability to use O_2 as the oxidant source.^{3*a*,⁴ Nevertheless, high methanol selectivity is only realized at very low conversion, because of the high susceptibility of methanol and other oxygenates to overoxidation under catalytic conditions.⁵ To overcome this conversion-selectivity constraint, one promising strategy introduced in homogeneous catalytic systems is to functionalize the primary product in the form of methyl esters, notably methyl bisulfate⁶ and methyl trifluoroacetate,⁷ which can be subsequently hydrolyzed to methanol. As a consequence of the high stability of the methyl ester in the reaction environment, these methane-to-methyl-ester (MTME) systems successfully break through the selectivity-conversion barrier that is}

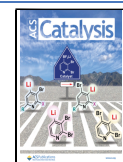
ubiquitous for direct-methane-to-methanol (DMTM) systems.⁸ Despite unprecedented yields, there remain several challenges for this chemistry, particularly the use of corrosive and concentrated acids, economically inviable oxidants (e.g., $\text{K}_2\text{S}_2\text{O}_8$, SO_3),⁹ and homogeneous catalysts.¹⁰ According to techno-economical evaluation, only the use of oxygen as the oxidant is viable.⁹ The transition to solid catalysts has been limited, although there are a few successful examples: Metals coordinated to porous organic polymers exhibit similar or even higher activity than their homogeneous analogues with SO_3 (oleum) or $\text{K}_2\text{S}_2\text{O}_8$ as oxidant.¹¹

This work is based on our newly developed aerobic, heterogeneous catalytic process that protects methanol via esterification to methyl trifluoroacetate under substantially milder reaction conditions in comparison to conventional homogeneous catalyzed systems.^{3*b*} Methane is partially oxidized by air over a solid catalyst and subsequently esterified to methyl trifluoroacetate in a reaction medium of trifluoroacetic acid (TFA) diluted with an inert perfluorohexane

Received: December 21, 2022

Revised: February 28, 2023

Published: March 4, 2023



cosolvent. After reaction, the produced methyl ester can be easily recovered through a facile liquid–liquid extraction with the polar aprotic solvent at ambient temperature, and the product concentration can be directly determined using ^1H NMR. Diluting TFA to more manageable concentrations of 10 wt % in the noncorrosive and oxidation-resistant perfluorohexane greatly reduces the corrosivity of the reaction medium and allows for operation in less-aggressive conditions that may improve the stability of a heterogeneous catalyst, and also facilitates the product recovery via extraction with a non-fluorous polar solvent. Moreover, the highly effective product separation method provides the possibility of recycling the fluorous cosolvent, representing a unique advantage of this system. We recently showed that cobalt-containing silica catalysts synthesized via incipient wetness impregnation (IWI) exhibit promising activity in this reaction system.³¹ In more conventional systems for the conversion of methane to methyl trifluoroacetate, many homogeneous transition-metal-based catalysts have been studied, especially those based on copper¹² and cobalt^{7a,13} salts. Still, the use of manganese-based catalysts for this reaction is more limited, even despite the advantage that manganese is one of the most cost-effective and abundant 3d transition metals, especially compared to cobalt.¹⁴ More than a decade prior, a manganese oxide precatalyst was first shown to have high activity (36% methane-based yield, >95% selectivity) for homogeneous conversion of methane to methyl trifluoroacetate using air as the oxidant, and, recently, a manganese trifluoroacetate salt was reported to be highly active in mixtures of TFA and trifluoroacetate anhydride.^{14a,e} The notable turnovers of up to 8.5 of these studies on homogeneous manganese catalysts for the production of methyl esters motivates further research into exploring manganese-based catalysts for methane partial oxidation applications. In this Letter, we aim to translate the high activity of molecular manganese catalysts to a heterogeneous mode using simple fabrication methods. We developed active solid manganese-containing catalysts for the MTME reaction that use air as the oxidant source under the improved reaction conditions, thereby demonstrating the potential of manganese as an active catalyst for methane conversion that has not been studied as extensively as other transition metals to date, despite its practical benefits. In addition to reporting the considerable activity of solid manganese-containing catalysts, the primary aim of this communication is to further the concept and development of suitable heterogeneous catalysts for the MTME reaction.

Herein, we synthesized manganese-based catalysts supported on silica gel, mesoporous silica, titania, and zirconia with varying manganese loadings via wet impregnation methods and evaluated their performance in methane partial oxidation in the batch system. After a screening of activity, the heterogeneity of the reaction for selected catalysts was assessed via ICP-OES and a hot filtration test of the reaction medium. EDXS of selected samples shows that the actual manganese loadings are generally comparable to the target values (Table S3 in the Supporting Information); therefore, productivities are calculated using the expected manganese loading based on the precursor amount as the basis. As can be seen in Table 1, as well as Figure S8a in the Supporting Information, silica-supported manganese catalysts substantially outperform titania- or zirconia-supported materials, in terms of overall ester productivity. While maximum ester productivity of $1068 \mu\text{mol g}_{\text{cat}}^{-1} \text{h}^{-1}$ is achieved with the 1.5 wt % Mn/SiO₂ catalyst,

Table 1. Screening of Catalytic Activity, Mn Leaching, and Hot-Filtration Test of Selected Manganese-Based Catalysts^a

entry	catalyst	methyl ester productivity [$\mu\text{mol g}_{\text{cat}}^{-1} \text{h}^{-1}$]	leached Mn ^b [mg]	hot filtration test ^c [%]
1	0.5 wt % Mn/SiO ₂	790	0.033 (6.5%)	9.7
2	1.5 wt % Mn/SiO ₂	1068	0.101 (6.7%)	8.7
3	5 wt % Mn/SiO ₂	990	1.418 (28.4%)	19.7
4	1.5 wt % Mn/SBA-15	1012	0.505 (33.7%)	—
5	1.5 wt % Mn/MCM-41	773	0.345 (23.0%)	—
6	5 wt % Mn/TiO ₂ -anatase	409	0.001 (0.02%)	—
7	10 wt % Mn/TiO ₂ -anatase	613	n.d.	n.d.
8	5 wt % Mn/TiO ₂ -rutile	380	n.d.	—
9	10 wt % Mn/TiO ₂ -rutile	510	n.d.	n.d.
10	10 wt % Mn/ZrO ₂	606	0.015 (0.1%)	—
11	5 wt % Mn/CeO ₂	1009	0.368 (7.4%)	—
12	1.5 wt % Mn/Al ₂ O ₃	311	0.059 (4.0%)	—
13	5 wt % Mn/Al ₂ O ₃	806	0.401 (8.0%)	—

^aReaction conditions: 100 mg of catalyst, 5 bar CH₄, 2 bar air, 10 g of 10 wt % TFA/C₆F₁₄ solution, 215 °C, 1 h. “—” denotes not measured; “n.d.” means not detected. ^bRelative leached Mn based on the theoretical loading is calculated in parentheses. ^cRelative increase in ester content based on that in the first run in the hot filtration test.

the ester productivity increases monotonically with increasing manganese loading up to $500\text{--}600 \mu\text{mol g}_{\text{cat}}^{-1} \text{h}^{-1}$ for the titania- and zirconia-supported catalysts. Generally, a common trend of decreasing manganese utilization efficiency with increasing metal loading is observed on all catalysts (see Figure S8b in the Supporting Information). In combination with the XRD and STEM results (see the Supporting Information), high dispersion of manganese oxide (MnO_x) is associated with high catalytic activity, in agreement with the general rule that dispersion positively affects the reducibility of supported MnO_x species.¹⁵ Accordingly, the most efficient manganese utilization of $352 \text{ mmol g}_{\text{Mn}}^{-1} \text{h}^{-1}$ ($19.4 \text{ mol mol}_{\text{Mn}}^{-1} \text{h}^{-1}$) is realized at the lowest loading on the silica support. Nevertheless, ICP-OES detected a considerable amount of leached manganese in the reaction filtrate with silica-supported catalysts, especially for high-loaded silica gel- and mesoporous silica-supported catalysts, whereas negligible metal leaching was found for all titania- and zirconia-supported catalysts (Figure S9 in the Supporting Information). Furthermore, significant homogeneous activity was observed in hot filtration tests with Mn/SiO₂ catalysts, which becomes more pronounced at higher manganese loading (from 10% to 20% increase in ester content; see Figure S10 in the Supporting Information). This result is in accordance with the amount of Mn leached from three catalysts (entries 1–3 in Table 1), indicating that the homogeneous activity is probably related to leached Mn species. In contrast, no increase in ester productivity is observed for both 10 wt % Mn/TiO₂ catalysts after removing

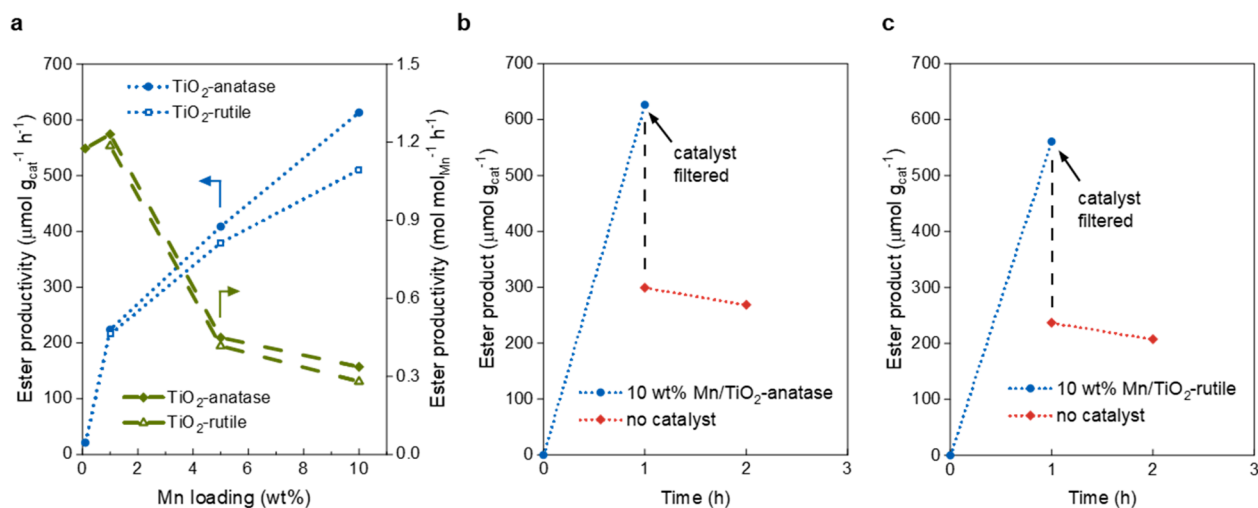


Figure 1. (a) Effect of manganese loading of Mn/TiO₂ catalyst on methyl trifluoroacetate productivity in methane oxidation. Reaction conditions: 100 mg of catalyst, 5 bar CH₄, 2 bar air, 10 g of 10 wt % TFA/C₆F₁₄ solution, 215 °C, 1 or 3 h (only for 0.1 wt % Mn/TiO₂). (b, c) Temporal evolution of MTFA during the initial methane oxidation reaction (blue) and hot filtration tests (red) with 10 wt % Mn/TiO₂. Reaction conditions: 100 mg of catalyst, 5 bar CH₄, 2 bar air, 10 g of 10 wt % TFA/C₆F₁₄ solution, 215 °C, catalyst filtered off after 1 h.

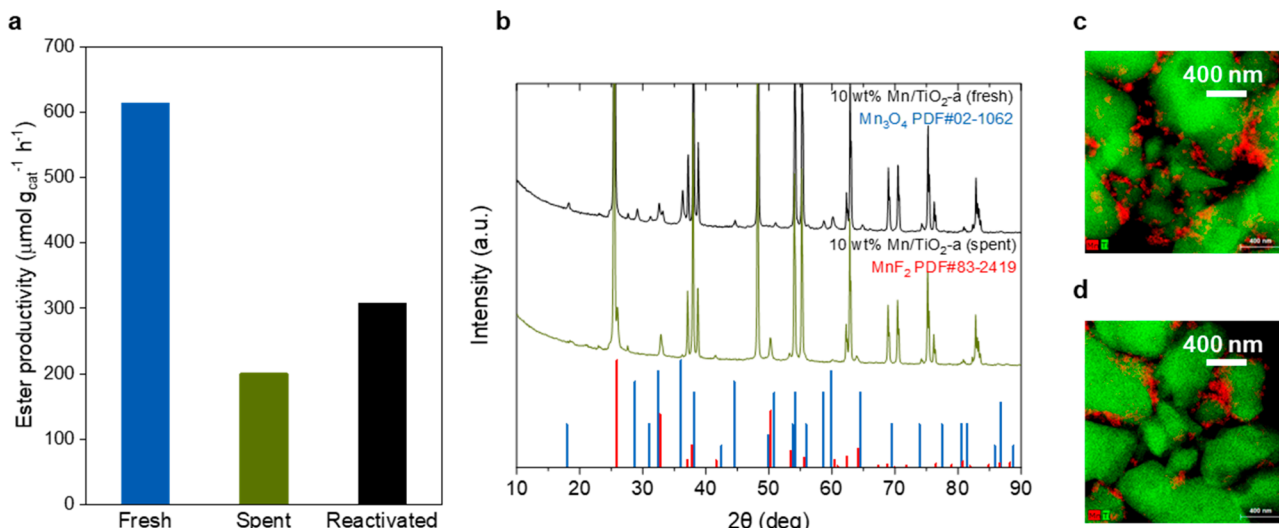


Figure 2. Mn/TiO₂ catalytic methane oxidation performance and characterization. (a) Methyl trifluoroacetate product obtained with fresh, spent, and reactivated 10 wt % Mn/TiO₂-anatase catalyst. Reaction conditions: 100 mg of catalyst, 5 bar CH₄, 2 bar air, 10 g of 10 wt % TFA/C₆F₁₄ solution, 215 °C, 1 h; (b) XRD patterns of fresh and spent 10 wt % Mn/TiO₂-anatase catalysts with Mn₃O₄ reference (blue, PDF No. 02-1062) and MnF₂ reference (red, PDF No. 83-2419); (c, d) STEM images of fresh and spent 5 wt % Mn/TiO₂-rutile catalysts (red for Mn, green for Ti) with scale bar = 400 nm, respectively.

the solid from the reaction medium (see Figures 1b and 1c, confirming the heterogeneity of the reaction. Because of their strict heterogeneity, productivity up to 613 $\mu\text{mol g}_{\text{cat}}^{-1} \text{h}^{-1}$ and apparent TOF up to 1.23 $\text{mol mol}_{\text{Mn}}^{-1} \text{h}^{-1}$), we selected the Mn/TiO₂ catalysts for further investigation.

As illustrated in Figure 1a, anatase- and rutile-supported manganese catalysts behave comparably concerning activity and manganese utilization. Increasing the manganese content of the anatase-supported catalysts from 1 wt % to 10 wt % results in a gradual increase in the ester productivity from 224 to 613 $\mu\text{mol g}_{\text{cat}}^{-1} \text{h}^{-1}$ (Figure 1a, blue markers), while rutile-supported catalysts are slightly less active at higher loadings (510 $\mu\text{mol g}_{\text{cat}}^{-1} \text{h}^{-1}$ at 10 wt %). Additionally, manganese utilization decreases rapidly with increasing manganese loading from 1 wt % to 10 wt % (Figure 1a, green markers). To further explore the manganese-based productivity in the low loading

range, 0.1 wt % Mn/TiO₂-anatase was also tested, giving an ester productivity of 21 $\mu\text{mol g}_{\text{cat}}^{-1} \text{h}^{-1}$, corresponding to 1.18 $\text{mol mol}_{\text{Mn}}^{-1} \text{h}^{-1}$ (Figure 1a). This manganese-based productivity is essentially equivalent to that achieved at a 1 wt % loading (1.23 $\text{mol mol}_{\text{Mn}}^{-1} \text{h}^{-1}$). This suggests that a further decrease in manganese loading below 1% on this support will not improve metal utilization, likely as a result of the well-dispersed manganese and lack of substantial aggregates present at and below 1 wt %. It is promising that almost no leached manganese was detected in the reaction filtrate for these catalysts, even at a high manganese loading of 10 wt % (see entries 7 and 9 in Table 1), indicative of the stability of MnO_x phases on titania during reaction, which significantly surpasses that of silica-supported catalysts. Moreover, the hot filtration test with 10 wt % Mn/TiO₂ shows that the reaction terminates after the filtration and removal of the solid catalyst (dotted red

curve, Figures 1b and 1c), thereby affirming the absence of active homogeneous species. In combination with the negligible leaching, the heterogeneous nature of the catalysis with Mn/TiO₂ catalysts can be confirmed.

To further examine the stability of the Mn/TiO₂ catalysts, 10 wt % Mn/TiO₂-anatase catalyst was recycled for a second run with and without an intermediate thermal treatment at 250 °C for 3 h in static air. We find neither the spent nor the reactivated catalyst can fully recover its original productivity achieved with the fresh catalyst (Figure 2a). The former demonstrates only one-third of the initial activity, while the latter is regenerated to half of the original value on the fresh catalyst. Since manganese leaching is negligible in these catalysts, and EDX further confirms that manganese content in the spent sample is close to the original loading (Table S3 in the Supporting Information), the decrease in activity could be attributed to other factors, such as structural change of the support, aggregation of MnO_x, or irreversible formation of an inactive phase could also negatively affect the activity and result in the deactivation of the catalyst. Herein, the XRD patterns and STEM images of fresh and spent Mn/TiO₂ catalysts are analyzed and compared in detail.

For fresh samples, all XRD spectra contain several sharp reflections corresponding to the pure anatase phase of titania (see Figure S14a in the Supporting Information) and the rutile phase of titania (Figure S14b in the Supporting Information), the relative intensity of which does not visibly change at different manganese loadings, indicating that the crystalline structure of the support was not observably altered after impregnation and calcination. Additional reflections assigned to the Mn₃O₄ phase are differentiable in samples with a manganese content of 5 and 10 wt %, and their intensity increases gradually with increasing manganese loading. Therefore, these samples mainly consist of a crystalline Mn₃O₄ phase of relatively large particle sizes. In addition, a few less intense reflections across all loadings are visible, which denote the presence of Mn₂O₃ and/or MnO₂. The STEM images of the fresh Mn/TiO₂ samples (Figure 2c and the Supporting Information) coincide with the observations in XRD, suggesting that MnO_x are poorly dispersed and form aggregated, large-sized particles for high-loaded samples (5 and 10 wt %), whereas Mn is relatively uniformly dispersed at 1 wt % loading, except for a few small aggregated particles. When combined with the similar manganese-based productivity between 0.1 and 1 wt % Mn/TiO₂, it appears that, below a certain loading, the same distribution of manganese species is maintained with an overall similar effective catalytic activity, while above this limit loading different distributions of manganese species with different activity play a role in catalyzing the conversion of methane. In this context, it could be speculated that if we further decrease the manganese loading, a linear relationship between the ester yield and the total catalyst/manganese mass would be expected. Overall, the dispersion state of MnO_x, together with the low BET surface areas of support (Table S2 in the Supporting Information), could be responsible for their distinct performance compared to SiO₂-supported catalysts. Thus, the WI method fails to uniformly disperse manganese on TiO₂, and the more so as the loading increases.

In comparison to fresh 10 wt % Mn/TiO₂ catalysts, most of the reflections specific to Mn₃O₄ become hardly observable in XRD patterns of spent samples (Figure 2b and Figure S14c in the Supporting Information), except for two resolved

reflections at 36.2° and 60.0° with very low intensity. Thus, the original Mn₃O₄ presumably undergoes a phase transition during the reaction. Several new reflections appear in the spectrum, among which the most intense reflections at $2\theta \approx 26^\circ$, 32.8° , and 50.4° can be assigned to the (110), (101), and (211) lattice plane of MnF₂. This observation reveals that the deactivation of catalysts probably results from the irreversible formation of MnF₂ and some mixed MnO_x phases containing manganese in the +2 state, which does not contribute to activity in methane oxidation under the reaction conditions.^{14a,e} Furthermore, no other patterns indicative of the formation of TiF_x or mixed Mn-TiO_x phases are observed, and the original reflections of both types of titania support remain the same, meaning that, after the reaction, the structure of the titania support was not affected. Consequently, the titania support is stable and resistant to the acidic and fluorous reaction environment. A comparison between STEM images of fresh and spent Mn/TiO₂ samples (Figures 2c and 2d, more images presented in the Supporting Information) indicates that a small number of manganese-containing particles may have undergone a small degree of local aggregation for 5 and 10 wt % Mn/TiO₂ catalysts, which appears to intensify the uneven manganese particle size distribution of these catalysts. Since the manganese loading varies greatly between different areas, it is difficult to determine the degree of particle aggregation after reaction. In contrast, manganese particles remain well-distributed in the spent 1 wt % Mn/TiO₂ sample and may even become better dispersed after reaction. Combined with XRD results, the manganese aggregates in spent 5 and 10 wt % samples consist of a mixture of oxide and fluoride phases, and both the formation of inactive MnF₂ and the possible particle size growth due to further manganese aggregates may account for the reduced activity of the recycled catalyst (Figure 2a). We note that, based on the heterogeneity of manganese distribution on these catalysts, there may be multiple manganese species active for the methane conversion reaction. Although Mn₃O₄ is determined to be the main phase on high-loading catalysts, the combination of catalytic activity and STEM points more to a correlation between high activity and dispersed manganese phases that cannot be as fully distinguished using the stated ex situ methods. Given the presence of multiple potentially active manganese species present on this catalyst, we note that the most active of the species has yet to be fully characterized and is the focus of future studies.

Through screening of supported manganese-based catalysts, we developed a titania-supported manganese catalyst that catalyzes the methane-to-methyl-trifluoroacetate process in diluted trifluoroacetic acid heterogeneously with high stability (minimal leaching of manganese) at a competitive activity (Table S4 in the Supporting Information). The presence of Mn₃O₄ as the major phase is confirmed on high-loading catalysts (5 and 10 wt %) by XRD, while STEM images indicate that manganese oxide exists in a poorly dispersed state on titania. Deactivation of the catalyst is partially attributed to the formation of inactive MnF₂ under reaction conditions. In contrast, high Mn dispersion was realized in the silica-supported catalyst that exhibited superior catalytic activity over Mn/TiO₂, but significant amounts of homogeneously active manganese were observed. XRD analysis pointed to a possible structural change of silica-based supports after reaction, which possibly accounted for the substantial leaching of manganese. Overall, high dispersion is of paramount

importance for achieving high activity in the catalytic system in this study, and the most efficient utilization of manganese is realized at lower loadings (<1%) in which manganese is highly dispersed on the support. On this basis, efforts should be taken to improve the manganese dispersion at higher loadings on the titania support in future work by employing higher surface area supports and alternative synthesis methods (e.g., coprecipitation). Besides, catalyst deactivation via formation of fluorides and other potential processes such as particle aggregation must be addressed. Multiple active manganese species may be present, and future studies to characterize in detail these species along with important interactions between manganese and the titania support are warranted. In summary, we demonstrate, for the first time, the potential of solid-supported manganese catalysts for this methane partial oxidation application. This development in employing a facilely synthesized solid manganese-containing catalyst to convert methane heterogeneously in satisfactory yield under improved conditions provides a promising approach for MTME systems and the movement toward more cost-effective and realistic catalysts for this process.

ASSOCIATED CONTENT

Supporting Information

The Supporting Information is available free of charge at <https://pubs.acs.org/doi/10.1021/acscatal.2c06292>.

Additional experimental details; materials and methods; NMR spectra; GC chromatogram; supplementary catalytic assessments, BET, EDXS, XRD and STEM characterization, UV-vis DR spectra, benchmark table ([PDF](#))

AUTHOR INFORMATION

Corresponding Author

Jeroen A. van Bokhoven – Institute for Chemistry and Bioengineering, ETH Zurich, 8093 Zürich, Switzerland; Laboratory for Catalysis and Sustainable Chemistry, Paul Scherrer Institut, 5232 Villigen, Switzerland;  orcid.org/0000-0002-4166-2284; Email: jeroen.vanbokhoven@chem.ethz.ch

Authors

Yinjie Ji – Institute for Chemistry and Bioengineering, ETH Zurich, 8093 Zürich, Switzerland

Andrea N. Blankenship – Institute for Chemistry and Bioengineering, ETH Zurich, 8093 Zürich, Switzerland;  orcid.org/0000-0003-3087-6719

Complete contact information is available at:

<https://pubs.acs.org/10.1021/acscatal.2c06292>

Author Contributions

All authors have given approval to the final version of the manuscript.

Notes

The authors declare no competing financial interest.

ACKNOWLEDGMENTS

This work was supported financially by ETH Zurich. The authors would also like to acknowledge Dr. Frank Krumeich (ETH Zurich) for his work in acquiring the electron microscopy images presented in this work.

REFERENCES

- (1) Clough, S. R. Methane. In *Encyclopedia of Toxicology*, Third Edition; Wexler, P., Ed.; Academic Press, 2014; pp 235–237.
- (2) (a) Bharadwaj, S. S.; Schmidt, L. D. Catalytic partial oxidation of natural gas to syngas. *Fuel Process. Technol.* **1995**, *42* (2), 109–127. (b) Lange, J.-P. Methanol synthesis: a short review of technology improvements. *Catal. Today* **2001**, *64* (1), 3–8. (c) Dybkjær, I.; Aasberg-Petersen, K. Synthesis gas technology large-scale applications. *Can. J. Chem. Eng.* **2016**, *94* (4), 607–612.
- (3) (a) Barbaux, Y.; Elamrani, A. R.; Payen, E.; Gengembre, L.; Bonnelle, J. P.; Grzybowska, B. Silica supported molybdena catalysts: Characterization and methane oxidation. *Appl. Catal.* **1988**, *44*, 117–132. (b) Spencer, N. D.; Pereira, C. J. V₂O₅/SiO₂-catalyzed methane partial oxidation with molecular oxygen. *J. Catal.* **1989**, *116* (2), 399–406. (c) Pannov, G. I.; Sobolev, V. I.; Kharitonov, A. S. The role of iron in N₂O decomposition on ZSM-5 zeolite and reactivity of the surface oxygen formed. *J. Mol. Catal.* **1990**, *61* (1), 85–97. (d) Panov, G. I.; Uriarte, A. K.; Rodkin, M. A.; Sobolev, V. I. Generation of active oxygen species on solid surfaces. Opportunity for novel oxidation technologies over zeolites. *Catal. Today* **1998**, *41* (4), 365–385. (e) Groothaert, M. H.; Smeets, P. J.; Sels, B. F.; Jacobs, P. A.; Schoonheydt, R. A. Selective oxidation of methane by the bis(mu-oxo)dicopper core stabilized on ZSM-5 and mordenite zeolites. *J. Am. Chem. Soc.* **2005**, *127* (5), 1394–1395. (f) Li, Y.; An, D.; Zhang, Q.; Wang, Y. Copper-Catalyzed Selective Oxidation of Methane by Oxygen: Studies on Catalytic Behavior and Functioning Mechanism of CuOx/SBA-15. *J. Phys. Chem. C* **2008**, *112* (35), 13700–13708. (g) Hammond, C.; Forde, M. M.; Ab Rahim, M. H.; Thetford, A.; He, Q.; Jenkins, R. L.; Dimitratos, N.; Lopez-Sanchez, J. A.; Dummer, N. F.; Murphy, D. M.; et al. Direct Catalytic Conversion of Methane to Methanol in an Aqueous Medium by using Copper-Promoted Fe-ZSM-5. *Angew. Chem., Int. Ed.* **2012**, *51* (21), 5129–5133. (h) Ab Rahim, M. H.; Forde, M. M.; Jenkins, R. L.; Hammond, C.; He, Q.; Dimitratos, N.; Lopez-Sanchez, J. A.; Carley, A. F.; Taylor, S. H.; Wilcock, D. J.; et al. Oxidation of Methane to Methanol with Hydrogen Peroxide Using Supported Gold–Palladium Alloy Nanoparticles. *Angew. Chem., Int. Ed.* **2013**, *52* (4), 1280–1284. (i) Narsimhan, K.; Iyoki, K.; Dinh, K.; Roman-Leshkov, Y. Catalytic Oxidation of Methane into Methanol over Copper-Exchanged Zeolites with Oxygen at Low Temperature. *ACS Central Sci.* **2016**, *2* (6), 424–429. (j) Zuo, Z.; Ramírez, P. J.; Senanayake, S. D.; Liu, P.; Rodriguez, J. A. Low-Temperature Conversion of Methane to Methanol on CeO_x/Cu₂O Catalysts: Water Controlled Activation of the C–H Bond. *J. Am. Chem. Soc.* **2016**, *138* (42), 13810–13813. (k) Tabor, E.; Dedecek, J.; Mlekodaj, K.; Sobalik, Z.; Andrikopoulos, P. C.; Sklenak, S. Dioxygen dissociation over man-made system at room temperature to form the active α -oxygen for methane oxidation. *Sci. Adv.* **2020**, *6* (20), No. eaaz9776. (l) Blankenship, A. N.; Ravi, M.; Newton, M. A.; van Bokhoven, J. A. Heterogeneously Catalyzed Aerobic Oxidation of Methane to a Methyl Derivative. *Angew. Chem., Int. Ed.* **2021**, *60* (33), 18138–18143. (m) Sun, L.; Wang, Y.; Wang, C.; Xie, Z.; Guan, N.; Li, L. Water-involved methane-selective catalytic oxidation by dioxygen over copper zeolites. *Chem.* **2021**, *7* (6), 1557–1568.
- (4) (a) Groothaert, M. H.; Smeets, P. J.; Sels, B. F.; Jacobs, P. A.; Schoonheydt, R. A. Selective Oxidation of Methane by the Bis(μ -oxo)dicopper Core Stabilized on ZSM-5 and Mordenite Zeolites. *J. Am. Chem. Soc.* **2005**, *127* (5), 1394–1395. (b) Tomkins, P.; Mansouri, A.; Bozbag, S. E.; Krumeich, F.; Park, M. B.; Alayon, E. M. C.; Ranocchiari, M.; van Bokhoven, J. A. Isothermal Cyclic Conversion of Methane into Methanol over Copper-Exchanged Zeolite at Low Temperature. *Angew. Chem., Int. Ed.* **2016**, *55* (18), 5467–5471. (Accessed Aug. 19, 2022.)
- (5) (a) Ahlquist, M.; Nielsen, R. J.; Periana, R. A.; Goddard, W. A. Product Protection, the Key to Developing High Performance Methane Selective Oxidation Catalysts. *J. Am. Chem. Soc.* **2009**, *131* (47), 17110–17115. (b) Ravi, M.; Ranocchiari, M.; van Bokhoven, J. A. The Direct Catalytic Oxidation of Methane to Methanol-A Critical Assessment. *Angew. Chem. Int. Ed.* **2017**, *56* (52), 16464–16483.

- (c) Latimer, A. A.; Kakekhani, A.; Kulkarni, A. R.; Norskov, J. K. Direct Methane to Methanol: The Selectivity-Conversion Limit and Design Strategies. *ACS Catal.* **2018**, *8* (8), 6894–6907. (d) Jovanovic, Z. R.; Lange, J.-P.; Ravi, M.; Knorpp, A. J.; Sushkevich, V. L.; Newton, M. A.; Palagin, D.; van Bokhoven, J. A. Oxidation of methane to methanol over Cu-exchanged zeolites: Scientia gratia scientiae or paradigm shift in natural gas valorization? *J. Catal.* **2020**, *385*, 238–245.
- (6) (a) Periana, R. A.; Taube, D. J.; Evitt, E. R.; Loffler, D. G.; Wentzcek, P. R.; Voss, G.; Masuda, T. A Mercury-Catalyzed, High-Yield System for the Oxidation of Methane to Methanol. *Science* **1993**, *259* (5093), 340–343. (b) Periana, R. A.; Taube, D. J.; Gamble, S.; Taube, H.; Satoh, T.; Fujii, H. Platinum catalysts for the high-yield oxidation of methane to a methanol derivative. *Science* **1998**, *280* (5363), 560–564.
- (7) (a) Vargaftik, M. N.; Stolarov, I. P.; Moiseev, I. I. Highly selective partial oxidation of methane to methyl trifluoroacetate. *J. Chem. Soc., Chem. Commun.* **1990**, *15*, 1049–1050. (b) Kao, L. C.; Hutson, A. C.; Sen, A. Low-temperature, palladium(II)-catalyzed, solution-phase oxidation of methane to methanol derivative. *J. Am. Chem. Soc.* **1991**, *113* (2), 700–701. (c) Sen, A.; Benvenuto, M. A.; Lin, M.; Hutson, A. C.; Basickes, N. Activation of methane and ethane and their selective oxidation to the alcohols in protic media. *J. Am. Chem. Soc.* **1994**, *116* (3), 998–1003. (d) Muehlhofer, M.; Strassner, T.; Herrmann, W. A. New Catalyst Systems for the Catalytic Conversion of Methane into Methanol. *Angew. Chem., Int. Ed.* **2002**, *41* (10), 1745–1747.
- (8) Ravi, M.; Sushkevich, V. L.; Knorpp, A. J.; Newton, M. A.; Palagin, D.; Pinar, A. B.; Ranocchiari, M.; van Bokhoven, J. A. Misconceptions and challenges in methane-to-methanol over transition-metal-exchanged zeolites. *Nat. Catal.* **2019**, *2* (6), 485–494.
- (9) Lange, J.-P. Economics of Alkane Conversion. In *Sustainable Strategies for the Upgrading of Natural Gas: Fundamentals, Challenges, and Opportunities*, Vol. 191; Derouane, E. G., Parmon, V., Lemos, F., Ramôa Ribeiro, F., Eds.; Springer: Dordrecht, The Netherlands, 2005; Chapter 3, pp 51–83.
- (10) Blankenship, A. N.; Ravi, M.; van Bokhoven, J. A. Esterification Product Protection Strategies for Direct and Selective Methane Conversion. *Chimia (Aarau)* **2021**, *75* (4), 305–310.
- (11) (a) Palkovits, R.; Antonietti, M.; Kuhn, P.; Thomas, A.; Schüth, F. Solid Catalysts for the Selective Low-Temperature Oxidation of Methane to Methanol. *Angew. Chem., Int. Ed.* **2009**, *48* (37), 6909–6912. (b) Zhang, Y.; Zhang, M.; Han, Z.; Huang, S.; Yuan, D.; Su, W. Atmosphere-Pressure Methane Oxidation to Methyl Trifluoroacetate Enabled by a Porous Organic Polymer-Supported Single-Site Palladium Catalyst. *ACS Catal.* **2021**, *11* (3), 1008–1013.
- (12) (a) Ravi, M.; van Bokhoven, J. A. Homogeneous Copper-Catalyzed Conversion of Methane to Methyl Trifluoroacetate in High Yield at Low Pressure. *ChemCatChem.* **2018**, *10* (11), 2383–2386. (b) Yin, G.; Piao, D.-g.; Kitamura, T.; Fujiwara, Y. Cu(OAc)₂-catalyzed partial oxidation of methane to methyl trifluoroacetate in the liquid phase. *Appl. Organomet. Chem.* **2000**, *14* (8), 438–442. (c) Ingrosso, G.; Midollini, N. Palladium (II)-or copper (II)-catalysed solution-phase oxyfunctionalisation of methane and other light alkanes by hydrogen peroxide in trifluoroacetic anhydride. *J. Mol. Catal. A: Chem.* **2003**, *204*–*205*, 425–431. (d) Liu, L. Y.; Fan, W.; Chen, W.; Chen, X. Y.; Li, S. H. KF-Promoted copper-catalyzed highly efficient and selective oxidation of methane and other alkanes with a dramatic additive effect. *Catal. Sci. Technol.* **2021**, *11* (14), 4962–4968.
- (13) Strassner, T.; Ahrens, S.; Muehlhofer, M.; Munz, D.; Zeller, A. Cobalt-Catalyzed Oxidation of Methane to Methyl Trifluoroacetate by Dioxygen. *Eur. J. Inorg. Chem.* **2013**, *2013* (21), 3659–3663.
- (14) (a) Chen, W. S.; Kocal, J. A.; Brandvold, T. A.; Bricker, M. L.; Bare, S. R.; Broach, R. W.; Greenlay, N.; Popp, K.; Walenga, J. T.; Yang, S. S.; et al. Manganese oxide catalyzed methane partial oxidation in trifluoroacetic acid: Catalysis and kinetic analysis. *Catal. Today* **2009**, *140* (3–4), 157–161. (b) Gandeepan, P.; Müller, T.; Zell, D.; Cera, G.; Warratz, S.; Ackermann, L. 3d Transition Metals for C–H Activation. *Chem. Rev.* **2019**, *119* (4), 2192–2452. (c) Li, M.; Lu, J. Cobalt in lithium-ion batteries. *Science* **2020**, *367* (6481), 979–980. (d) Mlekodaj, K.; Lemishka, M.; Sklenak, S.; Dedecek, J.; Tabor, E. Dioxygen splitting at room temperature over distant binuclear transition metal centers in zeolites for direct oxidation of methane to methanol. *Chem. Commun.* **2021**, *57* (28), 3472–3475. (e) Coutard, N.; Musgrave, C. B.; Moon, J.; Liebov, N. S.; Nielsen, R. M.; Goldberg, J. M.; Li, M.; Jia, X.; Lee, S.; Dickie, D. A.; et al. Manganese Catalyzed Partial Oxidation of Light Alkanes. *ACS Catal.* **2022**, *12* (9), 5356–5370.
- (15) Arena, F.; Torre, T.; Raimondo, C.; Parmaliana, A. Structure and redox properties of bulk and supported manganese oxide catalysts. *Phys. Chem. Chem. Phys.* **2001**, *3* (10), 1911–1917.

□ Recommended by ACS

Surface Oxygen Vacancy and Hydride Species on Ceria Are Detrimental to Acetylene Semihydrogenation Reaction

Zhaorui Li, Weixin Huang, et al.

MARCH 31, 2023
ACS CATALYSIS

READ ▶

Acid Catalysis over Crystalline Zr₃SO₄: Role of the Local Structure in Generating Acidity

Meilin Tao, Wataru Ueda, et al.

MARCH 20, 2023
ACS CATALYSIS

READ ▶

Base- and Additive-Free Carbon Dioxide Hydroboration to Methoxyboranes Catalyzed by Non-Pincer-Type Mn(I) Complexes

Sylwia Kostera, Luca Gonsalvi, et al.

MARCH 31, 2023
ACS CATALYSIS

READ ▶

Brønsted Acid Strength Does Not Change for Bulk and External Sites of MFI Except for Al Substitution Where Silanol Groups Form

Halley Balcom, David Hibbitts, et al.

MARCH 20, 2023
ACS CATALYSIS

READ ▶

Get More Suggestions >